horticulturae

MDPI

Article

Assessing the Potential of Sentinel-2 Derived Vegetation Indices to Retrieve Phenological Stages of Mango in Ghana

Benjamin Adjah Torgbor *, Muhammad Moshiur Rahman *, Andrew Robson, James Brinkhoff and Azeem Khan

Applied Agricultural Remote Sensing Centre, University of New England, Armidale, NSW 2351, Australia; arobson7@une.edu.au (A.R.); james.brinkhoff@une.edu.au (J.B.); azeemwsu@gmail.com (A.K.)

* Correspondence: btorgbor@myune.edu.au (B.A.T.); mrahma37@une.edu.au (M.M.R.); Tel.: +61-233(0)24-3131-459 (B.A.T.)

Abstract: In 2020, mango (*Mangifera indica*) exports contributed over 40 million tons, worth around US$20 billion, to the global economy. Only 10% of this contribution was made from African countries including Ghana, largely due to lower investment in the sector and general paucity of research into the mango value chain, especially production, quality and volume. Considering the global economic importance of mango coupled with the gap in the use of the remote sensing technology in the sector, this study tested the hypothesis that phenological stages of mango can be retrieved from Sentinel-2 (S2) derived time series vegetation indices (VIs) data. The study was conducted on four mango farms in the Yilo Krobo Municipal Area of Ghana. Seasonal (temporal) growth curves using four VIs (NDVI, GNDVI, EVI and SAVI) for the period from 2017 to 2020 were derived for each of the selected orchards and then aligned with five known phenology stages: Flowering/Fruitset (F/FS), Fruit Development (FRD), Maturity/Harvesting (M/H), Flushing (FLU) and Dormancy (D). The significance of the variation "within" and "between" farms obtained from the VI metrics of the S2 data were tested using single-factor and two-factor analysis of variance (ANOVA). Furthermore, to identify which specific variable pairs (phenology stages) were significantly different, a Tukey honest significant difference (HSD) post-hoc test was conducted, following the results of the ANOVA. Whilst it was possible to differentiate the phenological stages using all the four VIs, EVI was found to be the best related with $p < 0.05$ for most of the studied farms. A distinct annual trend was identified with a peak in June/July and troughs in December/January. The derivation of remote sensing based 'time series' growth profiles for commercial mango orchards supports the 'benchmarking' of annual and seasonal orchard performance and therefore offers a near 'real time' technology for identifying significant variations resulting from pest and disease incursions and the potential impacts of seasonal weather variations.

Keywords: mango (*Mangifera indica*); phenology; remote sensing; Sentinel-2 MSI; vegetation indices (VIs); Enhanced Vegetation Index (EVI); time series analysis

Citation: Torgbor, B.A.; Rahman, M.M.; Robson, A.; Brinkhoff, J.; Khan, A. Assessing the Potential of Sentinel-2 Derived Vegetation Indices to Retrieve Phenological Stages of Mango in Ghana. *Horticulturae* **2022**, *8*, 11. https://doi.org/10.3390/horticulturae8010011

Academic Editor: Esmaeil Fallahi

Received: 18 November 2021
Accepted: 17 December 2021
Published: 22 December 2021

1. Introduction

Mango (*Mangifera indica*) has been venerated as the 'King of Fruits' with a global production of 40 million tons at an average productivity of approximately 8 tons per ha from 5.4 million hectares [1,2]. The global annual economic value of mango exports in 2020 exceeded US$20 billion, with African countries contributing over 10% and 11% of global fresh and processed mango exports respectively [3,4]. The predominant commercial varieties grown globally include Tommy Atkins, Keitt and Kent. These varieties are preferred for their superior agronomic characteristics including low susceptibility to disease and pest infestation, ability to withstand damage during transportation, as well as sensory and visual appeal [5,6]. In Ghana, Keitt and Kent are predominantly grown due to their resistance to disease and availability during periods of high demand from importing nations [7,8]. The mango sector in Ghana is

rapidly expanding as a result of public and private sector initiatives to promote production, good agricultural practices, post-harvest processing and marketing systems [9]. Ghana's mango sector has a comparative advantage over other African countries in that, a greater part of the country has two harvest seasons with high quality mangoes which makes it suitable for fair-trade and organic niche markets [8–10]. As a result, mango is fast becoming one of the most important horticultural crops for export (like Cocoa) and for the domestic markets in Ghana [3,11,12]. However, compared to other producers such as India, Brazil and Mexico, mango productivity in Ghana remains very low [3,13] for several reasons including lack of research to determine optimal nutrient and pest management, low technology adoption and poor post-harvest handling practices among others [7]. Consequently, only about 15% of annual production output is of good quality for export [8]. Knowledge of crop growth stages, or phenology, is integral to proper management and yield improvement of mango crops [14]. Knowing the timing of the various phenology stages will ensure that farmers undertake the critical practices such as fertilization, pest and weed control and harvesting at the optimal time.

Phenology is the science of the synchronization of natural events and timing in crop development as influenced by weather variables such as rainfall, day length and temperature in its environment during certain seasons of the year [15]. A number of studies have classified mango crop phenology into five main stages including: Flowering/Fruitset (F/FS), Fruit Development (FRD), Maturity/Harvesting (M/H), Flushing (FLU) and Dormancy (D) [16,17]. The length of the period of each stage depends on a number of variables including weather conditions, location, variety, tree age and crop management. During the flowering stage, the mango tree produces large number of flowers which blossom all over the canopy, with colours ranging from white to brownish-red. It takes between one and three weeks for the petals of pollinated flowers to fall off and the stigma to form fruitlets, with non-pollinated stigma drying out [6]. Fruitlets formed at the fruitset stage increase in size during the fruit development stage of the physiological and phenological cycle. The fruit development stage lasts for 3 to 5 months [18]. Throughout the period of fruit development, both the leaves and fruits in most cases are green due to the presence of chlorophyll. Harvesting is done when the fruit is deemed physiologically mature but still hard and green to ensure there is sufficient time between harvesting and transportation to markets [10]. Pruning is usually done after harvesting to remove old branches, improve light interception and permit fresh leaf flush, which is a process of initiating vegetative growth of the resting buds on the branches of a tree canopy. Furthermore, dormancy is a period where growth of the mango tree stops. Technically, at this stage individual non-growing stems are resting, rendering the apical or lateral buds dormant [14]. It is a stage that is critical for flower induction [19]. The dormancy period normally takes 2 to 3 months. At the dormancy stage, the mango tree requires optimal water supply from rainfall or irrigation [19]. Even in similar environments, every stage of the mango's phenology, is heavily influenced by weather condition (temperature, atmospheric vapour pressure deficit and rainfall-water relation), nutrients and tree age [14,19].

Understanding the phenology of mango, particularly at varying scales (tree, orchard, regional and even national scale) offers significant benefit to the industry. At the grower level, understanding of phenology supports the identification of optimum timing for harvesting to maximize quality and inform harvesting logistics including labour, storage, transport etc. The application of crop inputs at key phenological stages for yield and quality forecasting is influenced by knowledge in crop phenology [20]. Establishing optimum harvesting timing is critical for mango, as an early harvest results in under ripe fruit that suffers poor eating qualities from reduced assimilation of sugars (reducing sweetness of the fruit), hard texture and green coloration (loss of blush) [21–26]. A delayed harvest results in the fruit ripening on the tree, making the flesh softer and therefore more susceptible to pest infestation and transport damage [22].

Consequently, the shelf life of the fruit is greatly reduced [23]. At the farm and regional scales, benchmarking historic phenology growth profiles against future seasons can enable specific constraints such as pest and disease to be quickly identified (i.e., rapid variations to historic averages). Similarly, seasonal variations associated with climate change can also be determined. Additionally, understanding crop phenological stages provides the agri-food industry and government organizations with vital information to better inform crop productivity forecasts in support of marketing and agricultural decision-making policy [27].

Previous studies have identified the use of remote sensing derived vegetation indices (VIs) for measuring a number of parameters in horticultural tree crops, including pigments, foliar nutrients, biomass and yield [1]. The approaches range from descriptive analysis to linear and non-linear regression modelling such as reflectance transformations and narrow band VIs [1], principal component analysis (PCA) [28,29]; and machine learning modelling approaches of the spectral data such as random forest (RF) [30,31], support vector machine (SVM) [32,33] and artificial neural network (ANN) [34] among others. Physically-based methods such as radiative transfer model (RTM) and inversions [35,36] and hybrid approaches that involve the combination of at least two of the methods have also been used previously [1]. Of all the approaches mentioned, the descriptive analysis and regression approach [37] have been widely used due to their simplicity, relative ease of application in crop monitoring and their sensitivity to crop phenological characteristics [38–41]. Their sensitivity to crop characteristics is largely due to the combination of two or more reflectance bands, capturing specific interactions between electromagnetic radiation and crop features including the concentration of chlorophyll and other pigments, leaf area as well as canopy biomass depending on the portion of the electromagnetic spectrum in use [38,40–43]. For example, decrease in chlorophyll concentration can represent plant senescence. Changes in chlorophyll concentration, therefore, are an indication of plant phenology, stress and developmental stage [44,45]. VIs such as NDVI, GNDVI, EVI and SAVI have been noted to be among the most critical indicators of vegetation phenology [46].

The increasing availability of remotely sensed data such as MODIS, SPOT, Landsat and Sentinel-2 [47] with high temporal resolution and long historic archives has provided greater analytical options in terms of mapping and modelling vegetation change seasonally and over time. Landsat series (4–8) have a global archive of satellite imagery starting from 1982 with spatial resolution of 30 m and revisit time of 16 days. However, considering the temporal resolution of Sentinel-2 with revisit time of 3 to 5 days and spatial resolution of 10 m for visible (Red, Green and Blue (RGB)) and near infrared (NIR) bands makes it a better choice for a time series analysis on mango phenology in cloud prone regions such as Ghana [48].

A number of studies have used remote sensing to characterize the phenology of both annual and perennial crops [14,15,49–51]. For example, Wang, et al. [31] applied a random forest algorithm to a Synthetic Aperture Radar (SAR) data to retrieve the phenology of four annual crop namely canola, corn, soybean and wheat, with Spearman correlation coefficients (R) of 0.93, 0.90, 0.85 and 0.91 respectively. Similarly, Zeng, et al. [49] demonstrated the ability of a hybrid approach in detecting the phenology of soybean and corn using a time-series MODIS data. Tedesco, et al. [37] used a combination of remote sensing derived VIs (NDVI, GNDVI and SAVI) and growing degree days (GDD) to characterize the phenology stages of sweet potato. In another study, Sawant, et al. [52] used NDVI time-series data obtained from Landsat archives spanning the period 1990–2015 to study the phenological growth stages and evapotranspiration of citrus. Furthermore, satellite image time series of Sentinel-1 and Sentinel-2 derived crop phenology was used to classify 9 perennial tree crops [53,54]. However, apart from the existing general paucity of research into satellite remote sensing of tree crops, specifically on mango crop phenology, there are several limitations including the use of low resolution satellite data as well as gap in the choice of crops with the earlier studies.

Given the economic importance of mango, particularly for countries such as Ghana and the non-existence of a study that applied remote sensing in retrieving its phenology, this current study tests the hypothesis that phenological stages of mango can be retrieved from Sentinel-2 derived time series VIs data. The study therefore aims at exploring the potential of freely available Sentinel-2 data to charcterize mango phenology stages in Ghana.

2. Materials and Methods

2.1. Study Area

The study was conducted in 4 farms (Table 1) within the Yilo Krobo Municipal area, near Somanya in the Eastern Region of Ghana (longitude 0°2′ E to 0°3′ W and latitude 6°2′ N to 6°4′ N), which accounts for more than 50% of the country's total mango production [7,8]. Ghana is a West African country located between Togo to the East, Cote D'Ivoire to the West, Burkina Faso to the North and the Gulf of Guinea to the South (Figure 1). The temperature in the study area ranges between a minimum of 24.9 °C and a maximum of 30 °C. Due to its location in the dry equatorial climatic zone, the annual rainfall ranges between 750 mm to 1600 mm. The area is characterized by a bi-modal rainfall season with the major rains in May/June and the minor rains in September/October. The farms used for the study are located on relatively flat lands with isolated undulating portions. The area is surrounded by hills on the northwestern ranges.

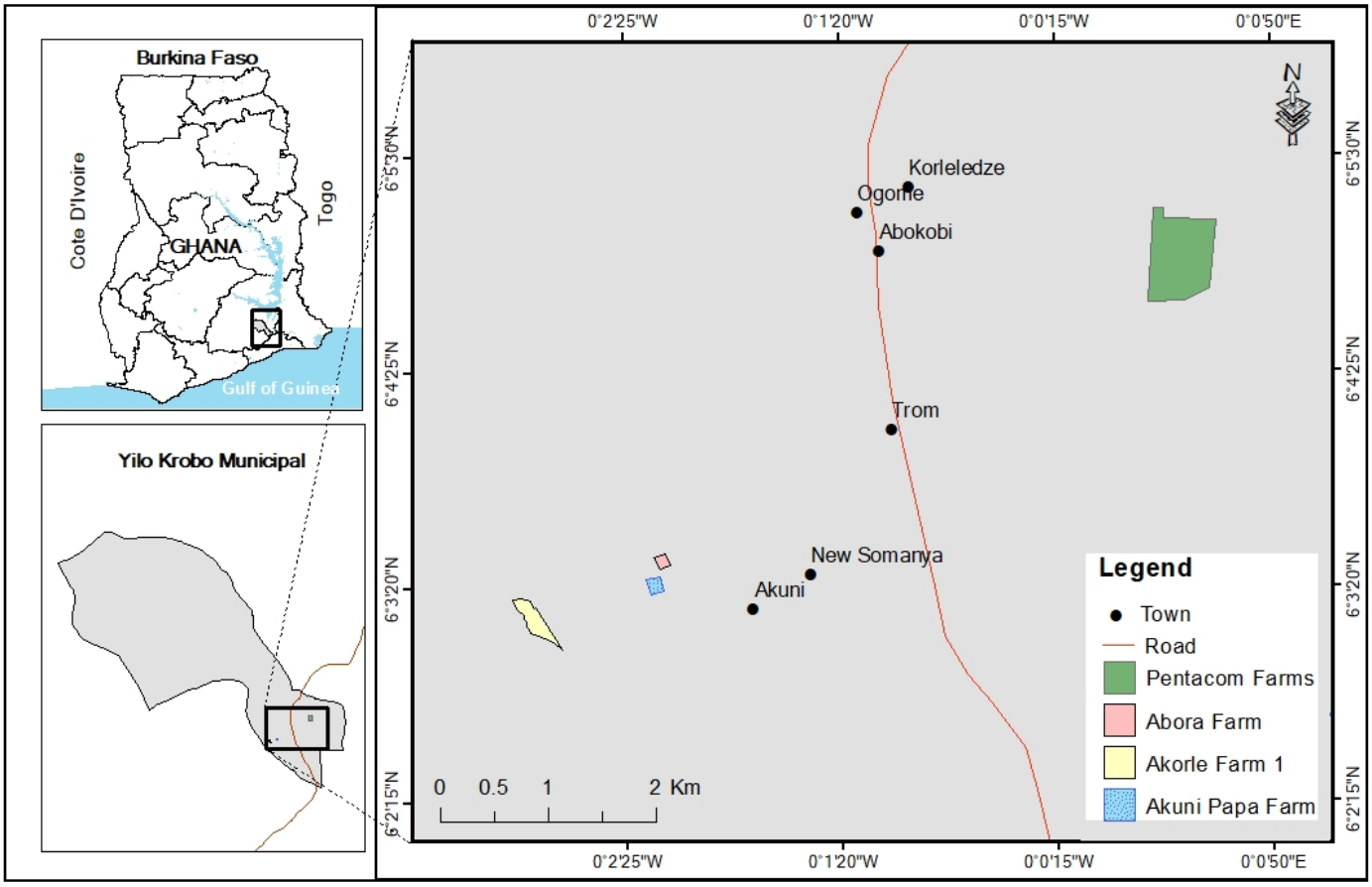

Figure 1. Study area map showing the four mango farms in the Yilo Krobo Municipal Area-Eastern Region, Ghana.

Table 1. Description of the four farms used in the study.

Name of Farm	Location	Ownership/ Management	Coordinate of Centroid	Tree Age (yr)	Size (ha)	Spacing (m)	Variety (%)
Pentacom Farms	Somanya	Corporate	0°0′22.045″ E 6°4′59.591″ N	18	45.0	10 × 8	Keitt (85), Kent and Others (15)
Abora Farm	Somanya	Small grower	0°2′14.438″ W 6°3′28.195″ N	18	1.3	10 × 10	Keitt (95), Kent (5)
Akuni Papa Farm	Somanya	Small grower	0°2′16.705″ W 6°3′20.774″ N	18	1.9	9 × 9	Keitt (95), Kent (5)
Akorle Farm 1	Somanya	Small grower	0°2′53.204″ W 6°3′10.632″ N	18	6.0	10 × 10	Keitt (95), Kent (5)

2.2. Data Acquisition and Processing

2.2.1. Mango Phenology Data

Data on the phenology and various farm management activities on the mango farms were obtained from the growers of all four farms over the 4-year period. This includes the dates physiological changes e.g., flowering, fruitset and leaf flush were first observed and farm management activities such as flower induction dates and harvesting were undertaken. Additionally, published literature relating to mango phenology cycles in Ghana and West Africa were reviewed [55,56]. The information indicated the growth stages and timings (Figure 2) where the collection of monthly satellite data was most required.

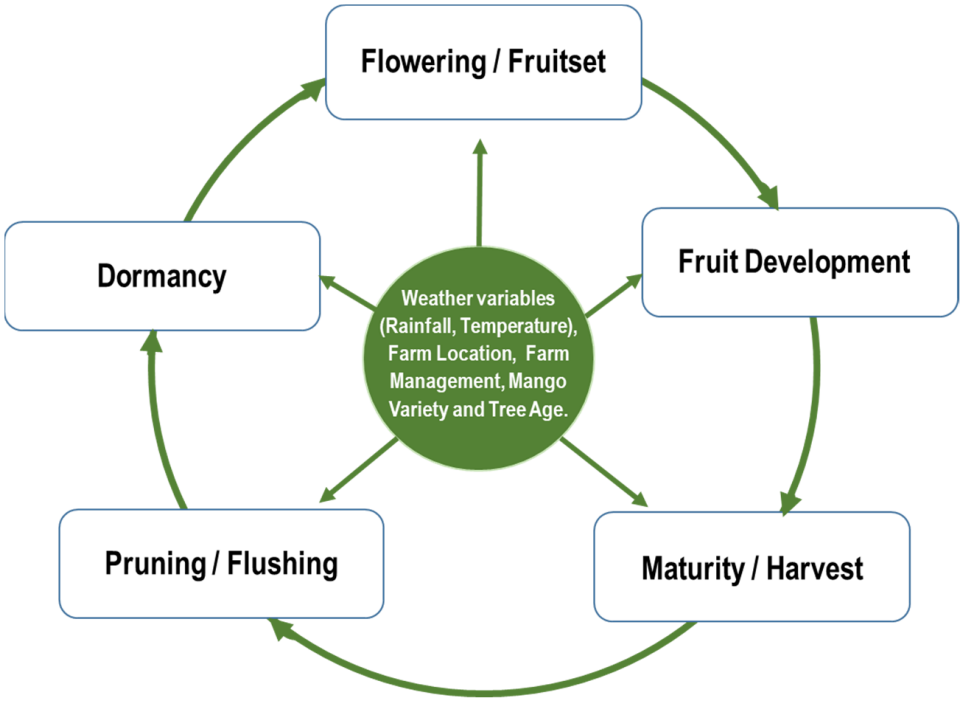

Figure 2. Main phenology stages of mango in Ghana.

For instance, since F/FS usually occur in January and February (J-F) in the southern part of Ghana (and other West African countries), all the available remote sensing data for those 2 months in a particular year were averaged and plotted. In similar manner, available images for the months of March, April and May (M-A-M) were averaged for the FRD stage. Images for June and July (J-J) were averaged to mark the M/H stage. On a few occasions, only a few images were useful for the J-J period. It is the time of

the year where there is a lot of cloud cover over the area, making it difficult to obtain a cloud free imagery. Furthermore, the FLU stage is observed in the months of August, September, October and November (ASON) and finally, the D stage occurs in December (D). The resulting aggregated remote sensing data was plotted to obtain the time series trend for the various farms over the 4-year period. All the median and maximum VI values at the various phenology stages within a year were averaged to obtain an annual temporal trend.

2.2.2. Extraction of Remote Sensing Data and Derivation of Vegetation Indices

Sentinel-2A (launched in June 2015) and Sentinel-2B (launched in March 2017) multi spectral (MS) data with a spatial resolution of 10 m for all visible and near infrared bands were acquired through the Digital Earth Africa (DE Africa) platform. It is a cloud-based platform with a repository of earth's observation SAR and optical data (including Landsat, Sentinel-1 and Sentinel-2) on which the analyst has the flexibility of conducting Remote Sensing analysis in a flexible and more efficient way by automating the various processes in computer-based codes in the digital Sandbox environment [57]. The platform provides an analysis-ready Level-2A (L2A) bottom of atmosphere (BOA) surface reflectance data, which is derived from level-1C (L1C) top of atmosphere (TOA) data using the Sen2Cor processor algorithm [58]. The algorithm is applied to mitigate the atmospheric effects on L1C data [59–61]. Sentinel-2 L2A data was acquired for 4 farms within the mango growing areas in the Yilo Krobo Municipal Area for full years, including 2017, 2018, 2019 and 2020. In total, 387 images were acquired for the analysis. A threshold was set for suitable images required for the time series analysis. All images with cloud cover 10% or less were considered suitable and were included in the analysis. From the $\leq$10% threshold filtered data, cloudy pixels found on the area of interest (farms) were masked out using the Fmask algorithm [62–64].

Two metrics, median and maximum for four vegetation indices (VIs) were extracted from polygon geometries defining the mango farm boundaries with 50 m buffer to correct for edge effect. The VIs studied were Normalized Difference Vegetation Index (NDVI) [65], Green Normalized Difference Vegetation Index (GNDVI) [66], Enhanced Vegetation Index (EVI) [67,68] and Soil Adjusted Vegetation Index (SAVI) [69]. These VIs have been used extensively for vegetation health and yield studies [70]. NDVI is effective for vegetation health study in areas with less biomass and leaf area index [50,71]. EVI is similar to NDVI and can also be used to quantify vegetation greenness. However, EVI is an optimized vegetation index that corrects for atmospheric conditions and canopy background noise and is more sensitive in areas with high biomass or dense vegetation [50,72,73]. EVI incorporates an "L" value to adjust for canopy background, "C" values as coefficients for atmospheric resistance, and values from the blue band (B). These enhancements allow for the ratio between the R and NIR values to be derived, while reducing the background noise, atmospheric noise, and saturation in most cases. Unlike NDVI and GNDVI which explore the chlorophyll content of the vegetation, EVI explores the structural characteristics of the plant and seeks to overcome the limitations of NDVI and GNDVI [40,47]. SAVI uses a transformation technique that minimizes the effect of soil brightness from VIs that use the Red and NIR wavelengths [50,71]. SAVI also incorporates an "L" value that corrects for soil background noise. Generally, L = 0 and L = 1 refers to high vegetation and no vegetation areas respectively. Due to the vegetation characteristics of the study area, an "L" value of 0.5 was applied [69,71].

The VIs are defined as:

$$\mathrm{NDVI} = \frac{\rho\mathrm{NIR} - \rho\mathrm{Red}}{\rho\mathrm{NIR} + \rho\mathrm{Red}} \quad (1)$$

$$\mathrm{GNDVI} = \frac{\rho\mathrm{NIR} - \rho\mathrm{Green}}{\rho\mathrm{NIR} + \rho\mathrm{Green}} \quad (2)$$

$$\mathrm{EVI} = \mathrm{G} \times \frac{\rho\mathrm{NIR} - \rho\mathrm{Red}}{\rho\mathrm{NIR} + \mathrm{C1} \times \rho\mathrm{Red} - \mathrm{C2} \times \rho\mathrm{Blue} + \mathrm{L}} \quad (3)$$

$$\text{SAVI} = \frac{\rho\text{NIR} - \rho\text{Red}}{\rho\text{NIR} + \rho\text{Red} + \text{L}}(1 + \text{L}) \quad (4)$$

where, ρNIR, ρBlue, ρGreen and ρRed refer to the reflectance in the Near-infrared ([B8] ~833 nm), Blue ([B2] ~493 nm), Green ([B3] ~560) and Red ([B4] ~665 nm) portions respectively of the electromagnetic spectrum. The values for the coefficients G, C1, C2 and L for EVI are 2.5, 6, 7.5 and 1 respectively. Additionally, the value of the constant L, in the SAVI formula is 0.5 after [69].

2.3. Data Analysis

To test for correlation among the VI metrics and the significance of the trends as well as variability within and between farms, descriptive data analysis including cross correlation, single-factor and two-factor analysis of variance (ANOVA) was undertaken using the Sentinel-2 data. The single-factor ANOVA was targeted at testing the relationship between the five phenology stages within farms. To identify which specific variable pairs (phenology stages) were significantly different, a Tukey honest significant difference (HSD) post-hoc test was conducted, following the results of the ANOVA. The Tukey's HSD test allows a simultaneous pairwise comparison of all the means of possible groups, to test for statistically significant difference between them [74]. Furthermore, the two-factor ANOVA was aimed at exploring the interactions of the various phenology stages between farms. The test was conducted using an online calculator [75]. Additionally, the phenology data from the four farms were compared with the remote sensing data. This was aimed at exploring the possibility of clearly differentiating the various phenology stages using remotely sensed VIs.

3. Results

3.1. Temporal Profiles of Remote Sensing Data at Key Phenological Stages

The extraction of the four vegetation indices from Sentinel-2 imagery over a four-year period (2017–2020) identified an annual growth profile with a peak in June/July and trough in December/January (Figure 3). Although the phenology stage characteristics of mango varied slightly from year to year for all the four farms, EVI_{med} proved to be consistently the best for differentiating the five phenology stages of mango in the study area. The temporal profile of mango phenology at the four farms is given in Figure 3. Less variation was observed in the Pentacom Farm (PF) and Akuni Papa Farms (APF) compared to those in the Abora (AF) and Akorle Farm 1 (AF1). The phenology curve for each farm had its own response to the VIs as shown in Figure 3. For instance, the variation around the mean EVI values for the Abora Farm was highest in the FRD, M/H and FLU stages followed by that of the Akorle Farm 1 over the 4-year period.

The bell-shaped EVI_{med} curve shows two stages on both sides of the "handle" which is the M/H. Taking the M/H stage of individual farms as center, the left sides of the curve have F/FS and FRD stages and right side have FLU and D completing the bell-shaped formation. The left side starts with a low EVI_{med} value from the F/FS stage and peaks with time through the FRD stage and terminates at the M/H stage. It then begins to trough through the FLU stages and ends the cycle at the D stages. This characteristic cycle of peaks and troughs occur annually, giving the Mango in the study area its phenology.

For each of the following farms the EVI temporal growth profiles are shown as EVI maximum values (EVI_{max}), EVI median values (EVI_{med}) and EVI yearly average values (EVI_{aa}). This demonstrates the average seasonal variability measure for each farm as well as the extremes in high and low reflectance (EVI) associated with seasonal, management or biotic/abiotic influences. The temporal profiles of all the four VI metrics (i.e., NDVI, GNDVI, EVI and SAVI) for the four farms (PF, AF, APF and AF1) can be found in the Supplementary Material (Figures S1–S4).

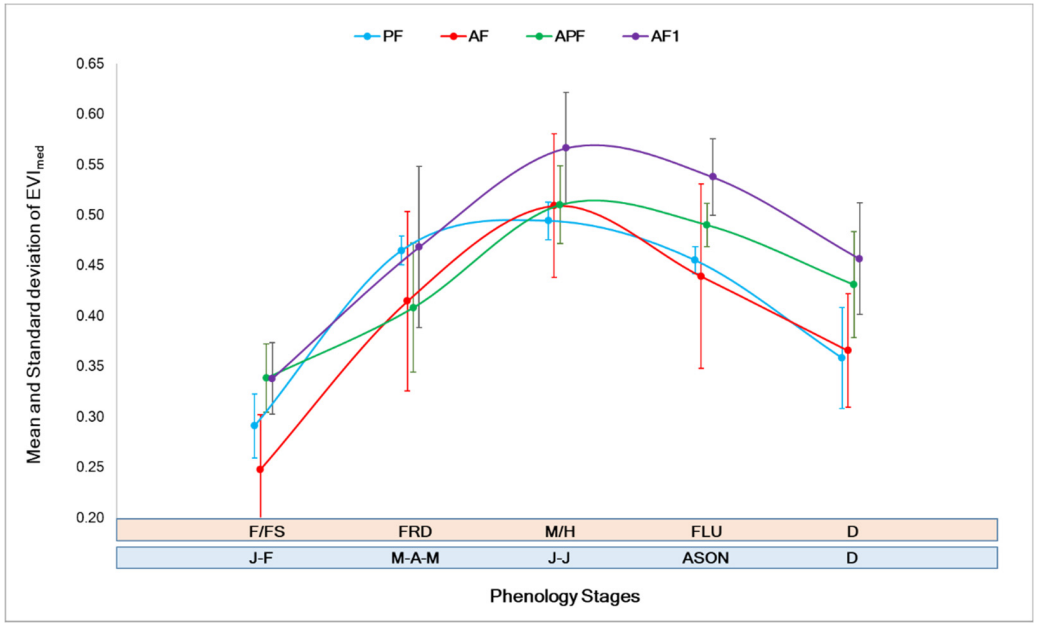

Figure 3. Overall mean and standard deviation of the four farms for the five phenology stages (F/FS, FRD, M/H, FLU and D) over the four years (2017–2020). *X*-axis offsets have been added to avoid overlapping error bars.

3.1.1. Pentacom Farm

The phenology characteristics of mango for Pentacom farm, in terms of date they occurred, did not show any considerable variation from year to year, therefore, the trend (and average of all the years in the time series) from 2017 to 2020 was similar for all the vegetation indices trialed. Temporal profile of mango phenology in relation to EVI metrics at the Pentacom farm is given in Figure 4. The lowest VIs_{med} were observed at the F/FS stage, whereas the peaks were observed at the M/H stage. For EVI_{max} the peak fluctuated in-between M/H and FLU. Additionally, the lowest EVI metrics were observed at the F/FS stage in 2020. Figure S1 shows the temporal profiles for NDVI, GNDVI and SAVI for the Pentacom Farm.

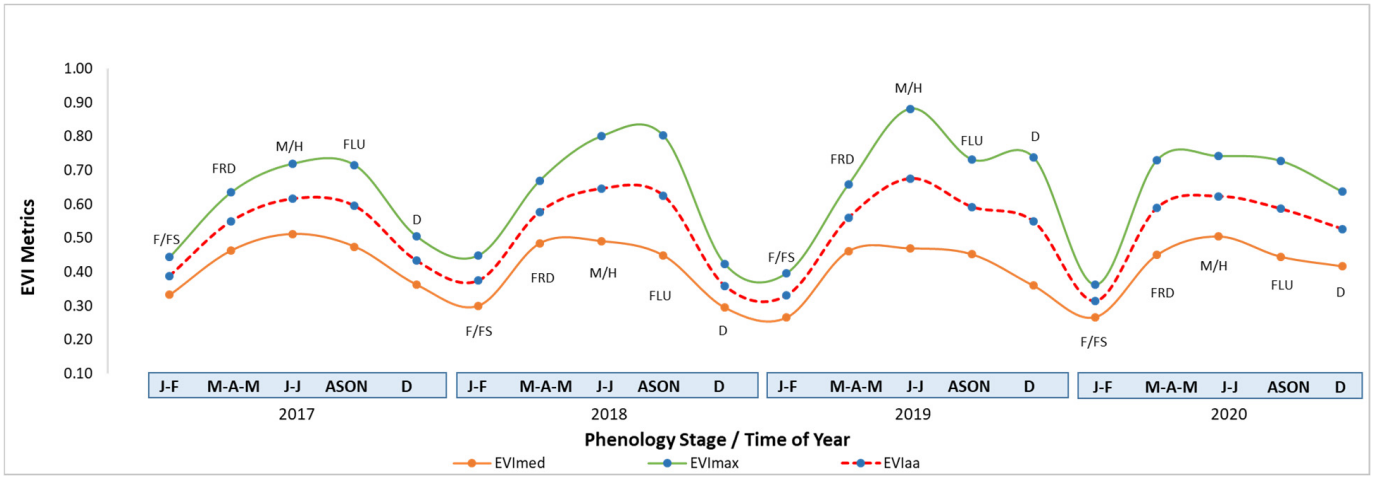

Figure 4. Temporal profile of mango in relation to the phenology cycle across the 4-year time series of median and maximum EVI metrics (EVI_{med}, EVI_{max}) together with their overall yearly average (EVI_{aa}) from the Pentacom Farm.

3.1.2. Abora Farm

There was a considerable variation in EVI metrics in the Abora Farm although similar trend of troughs around the F/FS and peaks at the M/H stages were observed across the time series. Thus generally, the highest EVI_{med} was recorded at the M/H stage of year 2017 with the lowest recorded in the F/FS stage of 2020. The EVI_{max} had a slight variation in 2018 and 2019 but generally, 2020 was the lowest across all the five phenology stages. Figure 5 shows the temporal profile of the EVI metrics at the various phenology stages in the Abora Farm. Figure S2 shows the temporal profiles for NDVI, GNDVI and SAVI for the Abora Farm.

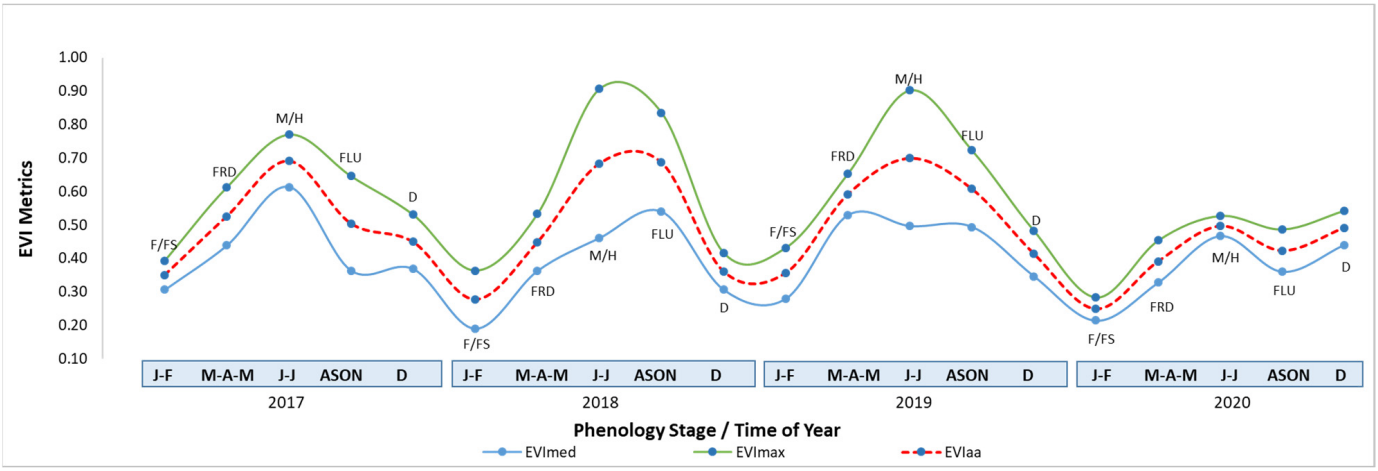

Figure 5. Temporal profile of mango in relation to the phenology cycle across the 4-year time series of median and maximum EVI metrics (EVI_{med}, EVI_{max}) together with their overall yearly average (EVI_{aa}) from the Abora Farm.

3.1.3. Akuni Papa Farm

There was no considerable variation in the phenology stages of mango in the Akuni Papa Farm across the time series (Figure 6). The FRD and M/H stages of 2017 showed a characteristic trough at the F/FS and peak at the M/H stages across the entire metrics of the VIs analyzed. EVI_{max} and EVI_{med} were lowest at the F/FS stage of 2020. Additionally, a slight trough and peak were observed at the M/H and FLU stages of 2018 for all the EVI metrics tested. Furthermore, EVI, to a large extent, showed the expected mango phenology trend, with the troughs at the F/FS stage and peaks at the M/H stage. Figure S3 shows the temporal profiles for NDVI, GNDVI and SAVI for the Akuni Papa Farm.

3.1.4. Akorle Farm 1

Generally, Akorle Farm 1 recorded the highest EVI_{med} compared to all the farms studied, mainly, from the F/FS to M/H stages of 2017. The lowest values were also largely recorded at the same stages in 2018 and 2020. EVI_{med} conformed appreciably well to the established phenology trend, with some variation. However, there exists some amount of fluctuation in the EVI_{max} between the M/H and FLU stages of 2017, 2018 and 2020. That is, unlike the EVI values at the M/H stage being generally higher than the FLU stage, to establish the expected trend, a slight trough was rather observed at the M/H stage of 2017, 2018 and 2020. Figure 7 shows the temporal profile of the EVI metrics for mango at the five phenology stages. Figure S4 shows the temporal profiles for NDVI, GNDVI and SAVI for the Akorle Farm 1.

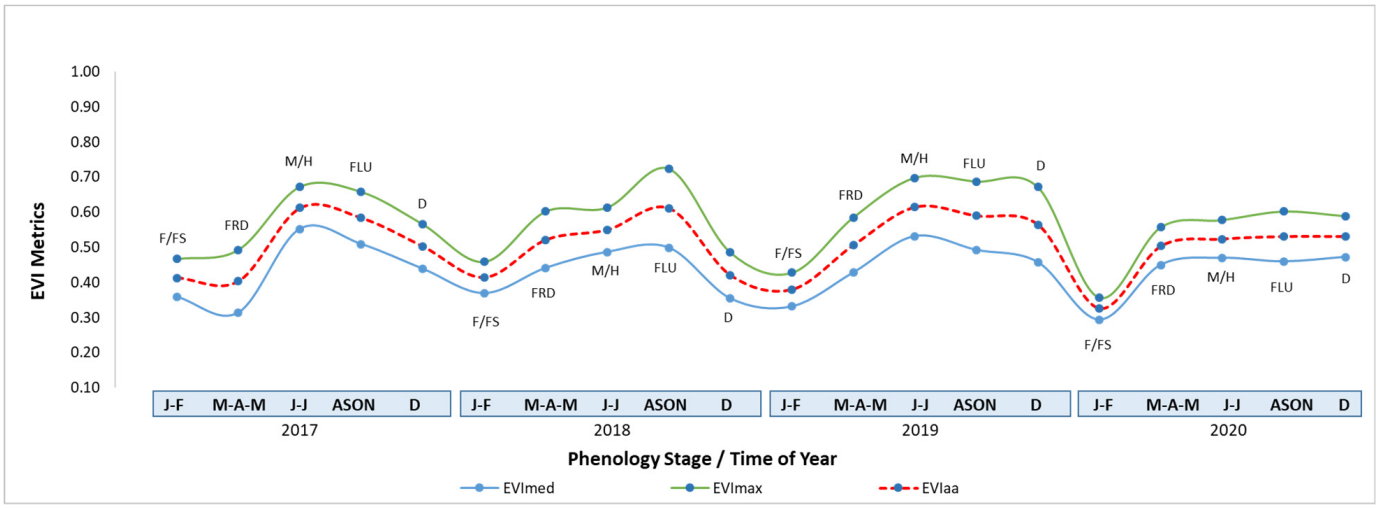

Figure 6. Temporal profile of mango in relation to the phenology cycle across the 4-year time series of median and maximum EVI metrics (EVI_{med}, EVI_{max}) together with their overall yearly average (EVI_{aa}) from the Akuni Papa Farm.

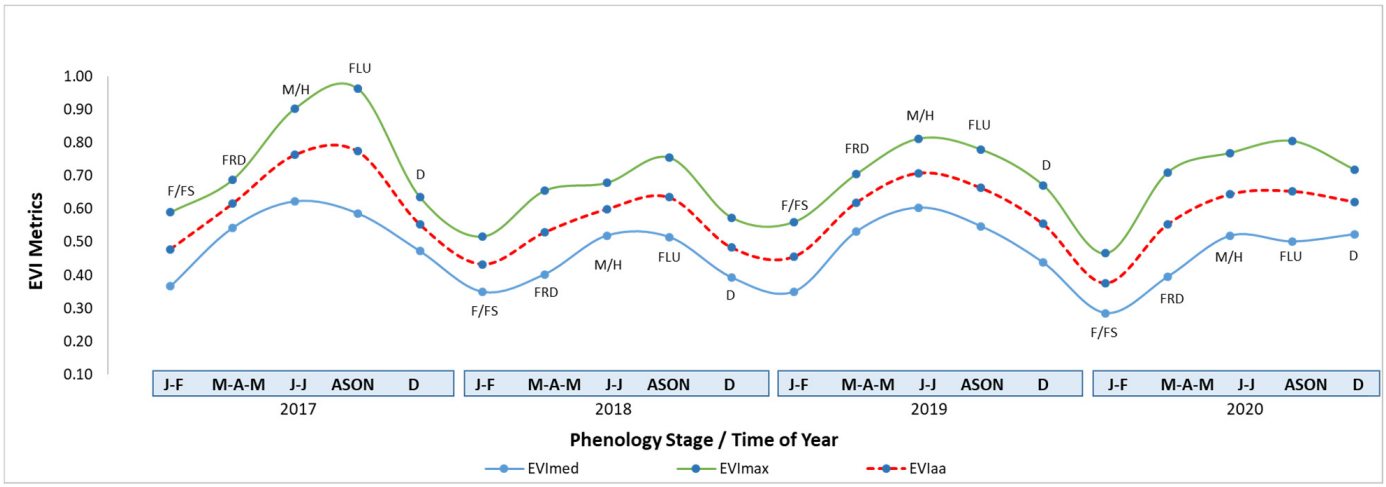

Figure 7. Temporal profile of mango in relation to the phenology cycle across the 4-year time series of median and maximum EVI metrics (EVI_{med}, EVI_{max}) together with their overall yearly average (EVI_{aa}) from the Akorle Farm 1.

3.2. Temporal Variability of Mango Phenology within Farms

The results of the Single-Factor ANOVA analysis (Table 2), in which "phenology stages" was the considered factor, suggests a significant variation at $p < 0.05$ within the four farms from most of the VIs trialed. The EVI metrics showed the most significant differences across all stages within the four farms. Overall, the results show on a farm-by-farm basis which phenology stages have equal means or otherwise to allow for the acceptance or rejection of the null hypothesis per the two VI metrics tested. For example, the results show that there was no significant difference between the means of the phenology stages in the Abora Farm and Akuni Papa Farm from the NDVI and GNDVI analysis.

Within all the farms, although the average trend in mango phenology from one stage to the other remained fairly stable, significant variation exists from year to year in the time series. Generally, there was less variation in EVI_{med} and EVI_{max} at the M/H stage across the time series. Observed EVI variation across the time series was rather found mostly at the D stage with EVI_{med} and EVI_{max} values ranging from 0.29–0.42 and 0.41–0.72 respectively.

Table 2. Results of a Single-Factor analysis of variance (ANOVA) of phenology stages within the four farms.

		NDVI Metrics		GNDVI Metrics		EVI Metrics		SAVI Metrics	
FARM	**Significance Test**	**Median**	**Maximum**	**Median**	**Maximum**	**Median**	**Maximum**	**Median**	**Maximum**
PF	*p*-value	0.0004	4.2×10^{-6}	0.0376	0.0013	2.3×10^{-7}	3.9×10^{-5}	5.3×10^{-5}	4.8×10^{-6}
AF	*p*-value	0.2752	2.2×10^{-1}	0.3068	0.1610	2.3×10^{-3}	1.8×10^{-3}	5.9×10^{-2}	3.5×10^{-2}
AF1	*p*-value	0.0017	4.7×10^{-7}	0.0040	0.0008	3.2×10^{-4}	2.3×10^{-4}	1.2×10^{-3}	1.6×10^{-4}
APF	*p*-value	0.2730	2.7×10^{-1}	0.3426	0.3480	5.1×10^{-4}	2.6×10^{-4}	2.1×10^{-2}	1.8×10^{-2}

The ANOVA test results generally showed a significant difference between means of the VIs of one or more phenology stages, leading to the rejection of the null hypothesis. However, information regarding which specific stages were significantly different from each other needs to be established. Therefore, a post-hoc test, the Tukey honest significant difference test was conducted, to show which phenological stages are significantly different from each other at $p < 0.01$ and $p < 0.05$ (Table 3).

Table 3. Results of the Tukey HSD test conducted on the phenology stages of the four farms.

FARM	**EVI METRIC**									
	EVI_{med}					**EVI_{max}**				
		F/FS	FRD	M/H	FLU	D	F/FS	FRD	M/H	FLU	D
Pentacom	F/FS										
	FRD	0.001 **					0.002 **				
	M/H	0.001 **	0.590				0.001 **	0.306			
	FLU	0.001 **	0.900	0.395			0.001 **	0.710	0.900		
	D	0.043 *	0.001 **	0.001 **	0.002 **		0.057	0.418	0.013 *	0.057	
Abora	F/FS										
	FRD	0.041 *					0.177				
	M/H	0.001 **	0.402				0.001 **	0.544			
	FLU	0.018 *	0.900	0.631			0.014 *	0.111	0.900		
	D	0.201	0.885	0.097	0.657		0.024 *	0.624	0.705	0.225	
Akuni Papa	F/FS										
	FRD	0.242					0.037 *				
	M/H	0.001 **	0.042 *				0.001 **	0.313			
	FLU	0.002 **	0.129	0.900			0.001 **	0.104	0.900		
	D	0.075	0.900	0.147	0.378		0.014 *	0.900	0.571	0.237	
Akorle Farm 1	F/FS										
	FRD	0.031 *					0.051				
	M/H	0.001 **	0.130				0.001 **	0.282			
	FLU	0.001 **	0.359	0.900			0.001 **	0.096	0.900		
	D	0.057	0.900	0.073	0.222		0.191	0.900	0.081	0.0235 *	

* significant at $p < 0.05$, ** significant at $p < 0.01$.

3.3. Temporal Variability of Mango Phenology between Farms

Variability in the mango crop characteristics in relation to the phenology stages between the four farms studied were explored. The relationship between mango farms and phenology stages was also tested. The *p*-values of the two-factor ANOVA (without replication) analyses on vegetation indices in relation to the phenology stages in the four farms are presented in Table 4. The results of the analysis show a significant variation at $p < 0.05$ between VIs and (1) the phenology stages (2) and the farms. This therefore allowed the rejection of the null hypothesis, that all phenology stages and mango farms have the same VIs mean values.

Table 4. Results of two-factor ANOVA analysis between the farms studied.

	NDVI		GNDVI		EVI		SAVI	
	Median	**Maximum**	**Median**	**Maximum**	**Median**	**Maximum**	**Median**	**Maximum**
Phenology Stage	3.1×10^{-6}	6.4×10^{-7}	3.2×10^{-6}	5.1×10^{-6}	4.4×10^{-7}	1.3×10^{-6}	2.4×10^{-7}	2.2×10^{-6}
Mango Farm	2.3×10^{-6}	9.8×10^{-7}	3.6×10^{-5}	9.5×10^{-5}	2.0×10^{-3}	1.5×10^{-3}	3.3×10^{-4}	5.1×10^{-4}

4. Discussion

Five main crop phenological stages were differentiated from this study which is consistent with the phenology stages observed by Vayssières, et al. [55]. These stages, namely F/FS, FRD, M/H, FLU and D occur yearly in the mango growing areas studied. There is a characteristic peak in June/July (M/H stage) and trough in December/January (D–F/FS stages) for the major production season. From a remote sensing perspective, reflectance measured by multispectral sensors are usually low at the flowering and fruitset stage compared to other stages in the phenological cycle due to the low chlorophyll content of the flowers. VIs values are relatively lower at this stage due to the lower reflectance in the NIR band which is chlorophyll sensitive [45]. Furthermore, considering the climate of Ghana, the flowering and fruitset period coincides with the peak of the dry season (December to February) where herbaceous vegetation growing in between the espacement of the mango tree mostly dry up. These situations may explain why the VIs value at the F/FS stage was low. Throughout the period of FRD, both the leaves and fruits are green due to the presence of chlorophyll. Therefore, high VIs values were obtained at the FRD stage compared to the F/FS stage in the left side of the bell-shaped curve. Furthermore, at the M/H stage, which is the peak of the growing season, what is measured by remote sensing sensors include mature fruits and other tree biomass as well as the grasses and herbaceous vegetation that may be favoured by the rains in Ghana around June/July. This results in the recording of higher VIs values at the M/H stage compared to all other stages. These production periods have been recognized and affirmed by Van Melle and Buschmann [10] and Zakari [8]. Subsequently, from the FLU stage (where pruning also occurs), the VIs values drop especially due to the general reduction of the biomass in the canopy through the removal of branches with leaves and the harvest of fruits [76,77]. Additionally, the new leaf flush does not contribute significant biomass to increase the reflectance or VIs values. This result in lower VIs values compared to the M/H stage which ends at the D stage [77].

Although variations exist within farms across the 4-year time series, EVI provided the consistently best VI relationship to the different phenology stages across the four farms. The results from the pairwise comparison (Table 3) show that different pairs (phenology stages) were retrieved from different farms. However, the F/FS–M/H and F/FS-FLU stages can be distinguished across all the farms at $p < 0.05$. This implies therefore that Sentinel-2 MS data derived VIs can be used to differentiate the F/FS–M/H and F/FS–FLU phenology stages on all the four mango farms. The significant variations

found within the farms, observed from the EVI, show that this metric may be used to clearly differentiate the phenology stages of mango on any of the farms within the study area. Hatfield and Hatfield and Prueger [50] used Simple ratio (SR), NDVI, EVI, SAVI, Chlorophyll green (CI_{green}), normalized pigment chlorophyll ratio (NPCI) and the plant senescence reflectance (PSRI) indices to differentiate phenology of soybean and six corn hybrids and explored the EVI as more promising in differentiating phenology stages due to its ability to overcome atmospheric and soil background noise, which is a challenge with the use of NDVI and GNDVI [50,78]. Moreover, as shown from a number of previous studies, EVI is more robust in the differentiation of the phenology stages due to its ability to explore the structural properties (branches, stems etc.) of the tree apart from just the leaves or green pigment [79–81]. Furthermore, the EVI metrics at the M/H stage of all the farms, showed relatively less seasonal variations within farms across the times series. This therefore presents a great opportunity for yield modelling in the studied farms [82].

Only few data points were available annually over the study sites especially from April to June/July due to continued cloud cover. This is a major challenge for optical satellite remote sensing in a tropical country such as Ghana. Results on phenology are usually unstable around this period although the trends are similar to what is expected. This variation in the metrics during the M/H stage of mango may be due to the limited availability of cloud free images over the farms particularly, in the months of June and July. In some cases, only one or two images are available in the months of June and July. This situation was overcome by interpolating values from available images. A potential solution to this time series-based problem could be the use of SAR data or the fusion of Sentinel-2 (10 m VNIR spatial resolution and 5 days revisit time) and PlanetScope data with 3 m spatial resolution and a daily revisit time [83]. This will provide a higher chance of successfully obtaining daily imagery during the cloudy days. Additionally, data for the study was available for only four years (2017–2020) which posed a significant limitation to this study. Data for more years (e.g., 10 or more from the Landsat Archives) could have been extremely useful in providing a better explanation in characterizing mango crop phenology. However, for small farms such as those used in the study, which is common in Ghana, the use of Landsat with a coarser spatial resolution, is challenging.

A number of factors including farm management and weather (rainfall and temperature) could have contributed largely to the variations in the phenology trends observed [82]. For example, in years 2019 and 2020 the erratic nature of the weather in the study area may have affected the phenology of mango. Specifically, massive rainfall was recorded in June 2019 and dropped significantly around the same time in the following year. However, the remote sensing derived VIs identified those variations in phenology comprehensively.

5. Conclusions

This study aimed to investigate the potential of S2 derived VIs to obtain information on five main crop phenology stages of mango, namely F/FS, FRD, M/H, FLU and D in Ghana. The study also underlined the spatial behaviour of mango crop phenology, temporal shifts with season and variation on farm level. Although the four VIs (NDVI, GNDVI, EVI and SAVI) tested show promise in differentiating the various crop phenology stages, EVI provided the consistently best VI to retrieve the different phenology stages across the four farms. The results of this study further revealed that the highest VI values were observed at the M/H stage while the lower values were recorded for the F/FS and D stages. Only two stages were distinguishable across all the four farms at $p < 0.05$ and the inter-annual variation in VIs was farm specific, with 2019 recording highest values for most farms. The alignment of satellite remote sensing derived VIs data to specific phenological growth stages offers great benefit to industry for guiding key timings for crop management activities including the application of crop inputs

(nutrition, growth regulators, fungicides inter alia) and harvest scheduling. These outputs thus support improved production and quality as well as the ongoing resilience and growth of Ghana's mango industry. It also provides the opportunity to relieve mango farmers of the stress in having to record farm operations and phenological events when they occur, by 'benchmarking' of annual and seasonal orchard performance for identifying significant variations resulting from pest and disease incursions and the potential impacts of seasonal weather variations. Although EVI showed promising results in identifying different phenological stages at most of the farms, further study would be required to affirm this claim. Recently, with the advent of very high-resolution imagery such as the PlanetScope with 3 m spatial resolution and a daily revisit time, this study can be further extended to predict the specific date of the mango crop phenology change. This will therefore provide valuable information for on farm crop management practices, developing yield prediction models and optimizing harvest logistics.

Supplementary Materials: The following are available online at https://www.mdpi.com/article/10.3390/horticulturae8010011/s1, Figure S1: Temporal profile of mango in relation to the phenology cycle across the 4-year time series of median (NDVImed, GNDVImed, EVImed and SAVImed) and maximum VI metrics (NDVImax, GNDVImax, EVImax and SAVImed) together with their overall yearly average (NDVIaa, GNDVIaa, EVIaa and SAVIaa) from the Pentacom Farm showing the five phenology stages differentiated including Flowering/Fruitset (F/FS), Fruit Development (FRD), Maturity/Harvesting (M/H), Flushing (FLU) and Dormancy (D), Figure S2: Temporal profile of mango in relation to the phenology cycle across the 4-year time series of median (NDVImed, GNDVImed, EVImed and SAVImed) and maximum VI metrics (NDVImax, GNDVImax, EVImax and SAVImed) together with their overall yearly average (NDVIaa, GNDVIaa, EVIaa and SAVIaa) from the Abora Farm showing the five phenology stages differentiated including F/FS, FRD, M/H, FLU and D, Figure S3: Temporal profile of mango in relation to the phenology cycle across the 4-year time series of median (NDVImed, GNDVImed, EVImed and SAVImed) and maximum metrics (NDVImax, GNDVImax, EVImax and SAVImed) together with their overall yearly average (NDVIaa, GNDVIaa, EVIaa and SAVIaa) from the Akuni Papa Farm showing the five phenology stages including F/FS, FRD, M/H, FLU and D, Figure S4: Temporal profile of mango in relation to the phenology cycle across the 4-year time series of median (NDVImed, GNDVImed, EVImed and SAVImed) and maximum metrics (NDVImax, GNDVImax, EVImax and SAVImed) together with their overall yearly average ($NDVI_{aa,}$ $GNDVI_{aa,}$ EVI_{aa} and $SAVI_{aa}$) from the Akorle Farm 1 showing the five phenology stages including F/FS, FRD, M/H, FLU and D.

Author Contributions: Conceptualization, B.A.T. and M.M.R.; methodology, B.A.T. and M.M.R.; writing—original draft preparation, B.A.T.; writing—review and editing, B.A.T., M.M.R., A.R., J.B. and A.K.; supervision, M.M.R., A.R., J.B. and A.K.; funding acquisition, A.R. All authors have read and agreed to the published version of the manuscript.

Funding: This study has been funded with support from a Remote Sensing scholarship granted by the Applied Agricultural Remote Sensing Centre (AARSC) of the University of New England, Australia.

Institutional Review Board Statement: Not applicable.

Informed Consent Statement: Not applicable.

Data Availability Statement: The data presented in this study are available on request from the corresponding authors.

Acknowledgments: The support of Abel Chemura, Edward Boamah and Victor Avah as well as managers and staff of Pentacom farm and Nkasst farms (owners of Abora Farm, Akuni Papa Farm and Akorle Farm 1) is highly acknowledged, for the invaluable contribution towards the success of this study.

Conflicts of Interest: The authors declare no conflict of interest.

References

1. Mahajan, G.R.; Das, B.; Murgaokar, D.; Herrmann, I.; Berger, K.; Sahoo, R.; Patel, K.; Desai, A.; Morajkar, S.; Kulkarni, R.M. Monitoring the Foliar Nutrients Status of Mango Using Spectroscopy-Based Spectral Indices and PLSR-Combined Machine Learning Models. *Remote Sens.* **2021**, *13*, 641. [CrossRef]
2. FAOSTAT. *Food and Agriculture Organization of the United Nations (FAO), FAO Statistic Database*; FAOSTAT: Rome, Italy, 2021.
3. Okorley, E.L.; Acheampong, L.; Abenor, M.T. The current status of mango farming business in Ghana: A case study of mango farming in the Dangme West District. *Ghana J. Agric. Sci.* **2014**, *47*, 73–80.
4. Altendorf, S. *Major Tropical Fruits Market Review 2017*; FAO: Rome, Italy, 2019; p. 10.
5. Evans, E.A.; Ballen, F.H.; Siddiq, M. Mango production, global trade, consumption trends, and postharvest processing and nutrition. In *Handbook of Mango Fruit*; John Wiley & Sons: Chichester, UK, 2017; pp. 1–16.
6. Litz, R.E. *The Mango: Botany, Production and Uses*; Cabi: Wallingford, UK, 2009.
7. Akotsen-Mensah, C.; Ativor, I.N.; Anderson, R.S.; Afreh-Nuamah, K.; Brentu, C.F.; Osei-Safo, D.; Boakye, A.A.; Avah, V. Pest Management Knowledge and Practices of Mango Farmers in Southeastern Ghana. *J. Integr. Pest Manag.* **2017**, *8*, 1–7. [CrossRef]
8. Zakari, A. *National Mango Study*; International Trade Center: Geneva, Switzerland, 2012.
9. Abu, M.; Olympio, N.; Darko, J.; Adu-Amankwa, P.; Dadzie, B. The mango industry in Ghana. *Ghana J. Hortic.* **2011**, *9*, 135–147.
10. van Melle, C.; Buschmann, S. Comparative analysis of mango value chain models in Benin, Burkina Faso and Ghana. In *Rebuilding West Africa's Food Potential*; FAO/IFAD: Rome, Italy, 2013.
11. Inkoom, E.W.; Micah, J.A. Estimating Economic Efficiency of Mango Production in Ghana. *ADRRI J. Agric. Food Sci.* **2017**, *3*, 29–46. Available online: http://www.journals.adrri.org/ (accessed on 2 December 2021).
12. Boakye-Yiadom, K.A.; Duca, D.; Pedretti, E.F.; Ilari, A. Environmental Performance of Chocolate Produced in Ghana Using Life Cycle Assessment. *Sustainability* **2021**, *13*, 6155. [CrossRef]
13. Yidu, P.K.D.; Dzorgbo, D. The State and Mango Export Crop Production in Ghana. *Ghana Soc. Sci. J.* **2016**, *13*, 185–208.
14. Ramirez, F.; Davenport, T.L.; Fischer, G.; Pinzón, J.C.A.; Ulrichs, C. Mango trees have no distinct phenology: The case of mangoes in the tropics. *Sci. Hortic.* **2014**, *168*, 258–266. [CrossRef]
15. Zhao, G.; Gao, Y.; Gao, S.; Xu, Y.; Liu, J.; Sun, C.; Liu, S.; Chen, Z.; Jia, L.; Gao, Y.; et al. The Phenological Growth Stages of Sapindus mukorossi According to BBCH Scale. *Forests* **2019**, *10*, 462. [CrossRef]
16. Delgado, P.M.H.; Aranguren, M.; Reig, C.; Galván, D.F.; Mesejo, C.; Fuentes, A.M.; Saúco, V.G.; Agustí, M. Phenological growth stages of mango (*Mangifera indica* L.) according to the BBCH scale. *Sci. Hortic.* **2011**, *130*, 536–540. [CrossRef]
17. Rajan, S.; Tiwari, D.; Singh, V.; Saxena, P.; Reddy, S.S.Y.; Upreti, K.; Burondkar, M.; Bhagwan, A.; Kennedy, R. Application of extended BBCH Scale for phenological studies in mango (*Mangifera indica* L.). *J. Appl. Hortic.* **2011**, *13*, 108–114. [CrossRef]
18. Siddiq, M.; Brecht, J.K.; Sidhu, J.S. *Handbook of Mango Fruit: Production, Postharvest Science, Processing Technology and Nutrition*; John Wiley & Sons: Hoboken, NJ, USA, 2017.
19. Whiley, A.W. Environmental Effects on Phenology and Physiology of Mango—A Review. *Acta Hortic.* **1993**, *341*, 168–176. [CrossRef]
20. Brunsell, N.; Pontes, P.P.B.; Lamparelli, R.A.C. Remotely Sensed Phenology of Coffee and Its Relationship to Yield. *GISci. Remote Sens.* **2009**, *46*, 289–304. [CrossRef]
21. Baloch, M.K.; Bibi, F. Effect of harvesting and storage conditions on the post harvest quality and shelf life of mango (*Mangifera indica* L.) fruit. *S. Afr. J. Bot.* **2012**, *83*, 109–116. [CrossRef]
22. Sivakumar, D.; Jiang, Y.; Yahia, E.M. Maintaining mango (*Mangifera indica* L.) fruit quality during the export chain. *Food Res. Int.* **2011**, *44*, 1254–1263. [CrossRef]
23. Gianguzzi, G.; Farina, V.; Inglese, P.; Rodrigo, M.G.L. Effect of Harvest Date on Mango (*Mangifera indica* L. Cultivar Osteen) Fruit's Qualitative Development, Shelf Life and Consumer Acceptance. *Agronomy* **2021**, *11*, 811. [CrossRef]
24. Jha, S.; Narsaiah, K.; Sharma, A.; Singh, M.; Bansal, S.; Kumar, R. Quality parameters of mango and potential of non-destructive techniques for their measurement—A review. *J. Food Sci. Technol.* **2010**, *47*, 1–14. [CrossRef]
25. Jha, S.; Kingsly, A.; Chopra, S. Physical and mechanical properties of mango during growth and storage for determination of maturity. *J. Food Eng.* **2006**, *72*, 73–76. [CrossRef]
26. Prasad, K.; Jacob, S.; Siddiqui, M.W. Fruit maturity, harvesting, and quality standards. In *Preharvest Modulation of Postharvest Fruit and Vegetable Quality*; Academic Press: Cambridge, MA, USA, 2018; pp. 41–69.
27. Ceglar, A.; van der Wijngaart, R.; de Wit, A.; Lecerf, R.; Boogaard, H.; Seguini, L.; Berg, M.V.D.; Toreti, A.; Zampieri, M.; Fumagalli, D.; et al. Improving WOFOST model to simulate winter wheat phenology in Europe: Evaluation and effects on yield. *Agric. Syst.* **2018**, *168*, 168–180. [CrossRef]
28. Mouazen, A.M.; Kuang, B.; De Baerdemaeker, J.; Ramon, H. Comparison among principal component, partial least squares and back propagation neural network analyses for accuracy of measurement of selected soil properties with visible and near infrared spectroscopy. *Geoderma* **2010**, *158*, 23–31. [CrossRef]
29. Krishna, G.; Sahoo, R.N.; Singh, P.; Bajpai, V.; Patra, H.; Kumar, S.; Dandapani, R.; Gupta, V.K.; Viswanathan, C.; Ahmad, T.; et al. Comparison of various modelling approaches for water deficit stress monitoring in rice crop through hyperspectral remote sensing. *Agric. Water Manag.* **2018**, *213*, 231–244. [CrossRef]

30. Chemura, A.; Mutanga, O.; Odindi, J. Empirical modeling of leaf chlorophyll content in coffee (coffea arabica) plantations with sentinel-2 msi data: Effects of spectral settings, spatial resolution, and crop canopy cover. *IEEE J. Sel. Top. Appl. Earth Obs. Remote Sens.* **2017**, *10*, 5541–5550. [CrossRef]
31. Wang, H.; Magagi, R.; Goïta, K.; Trudel, M.; McNairn, H.; Powers, J. Crop phenology retrieval via polarimetric SAR decomposition and Random Forest algorithm. *Remote Sens. Environ.* **2019**, *231*, 111234. [CrossRef]
32. Zhang, H.; Kang, J.; Xu, X.; Zhang, L. Accessing the temporal and spectral features in crop type mapping using multi-temporal Sentinel-2 imagery: A case study of Yi'an County, Heilongjiang province, China. *Comput. Electron. Agric.* **2020**, *176*, 105618. [CrossRef]
33. Küçük, Ç.; Taşkın, G.; Erten, E. Paddy-rice phenology classification based on machine-learning methods using multitemporal co-polar X-band SAR images. *IEEE J. Sel. Top. Appl. Earth Obs. Remote Sens.* **2016**, *9*, 2509–2519. [CrossRef]
34. Ye, X.; Sakai, K.; Garciano, L.O.; Asada, S.-I.; Sasao, A. Estimation of citrus yield from airborne hyperspectral images using a neural network model. *Ecol. Model.* **2006**, *198*, 426–432. [CrossRef]
35. Baret, F.; Weiss, M.; Troufleau, D.; Prevot, L.; Combal, B. Maximum information exploitation for canopy characterization by remote sensing. *Asp. Appl. Biol.* **2000**, *60*, 71–82.
36. Koetz, B.; Baret, F.; Poilvé, H.; Hill, J. Use of coupled canopy structure dynamic and radiative transfer models to estimate biophysical canopy characteristics. *Remote Sens. Environ.* **2005**, *95*, 115–124. [CrossRef]
37. Tedesco, D.; de Oliveira, M.F.; dos Santos, A.F.; Costa Silva, E.H.; de Souza Rolim, G.; da Silva, R.P. Use of remote sensing to characterize the phenological development and to predict sweet potato yield in two growing seasons. *Eur. J. Agron.* **2021**, *129*, 126337. [CrossRef]
38. Kawamura, K.; Mackay, A.; Tuohy, M.P.; Betteridge, K.; Sanches, I.; Inoue, Y. Potential for spectral indices to remotely sense phosphorus and potassium content of legume-based pasture as a means of assessing soil phosphorus and potassium fertility status. *Int. J. Remote Sens.* **2011**, *32*, 103–124. [CrossRef]
39. Darvishzadeh, R.; Skidmore, A.; Schlerf, M.; Atzberger, C.; Corsi, F.; Cho, M. LAI and chlorophyll estimation for a heterogeneous grassland using hyperspectral measurements. *ISPRS J. Photogramm. Remote Sens.* **2008**, *63*, 409–426. [CrossRef]
40. Huete, A.; Didan, K.; van Leeuwen, W.; Miura, T.; Glenn, E. MODIS vegetation indices. In *Land Remote Sensing and Global Environmental Change*; Springer: Berlin/Heidelberg, Germany, 2010; pp. 579–602.
41. Berger, K.; Verrelst, J.; Féret, J.-B.; Wang, Z.; Wocher, M.; Strathmann, M.; Danner, M.; Mauser, W.; Hank, T. Crop nitrogen monitoring: Recent progress and principal developments in the context of imaging spectroscopy missions. *Remote Sens. Environ.* **2020**, *242*, 111758. [CrossRef]
42. Ferwerda, J.G.; Skidmore, A.K.; Mutanga, O. Nitrogen detection with hyperspectral normalized ratio indices across multiple plant species. *Int. J. Remote Sens.* **2005**, *26*, 4083–4095. [CrossRef]
43. Lillesand, T.; Kiefer, R.W.; Chipman, J. *Remote Sensing and Image Interpretation*; John Wiley and Sons: Hoboken, NJ, USA, 2015.
44. Blackburn, G.A. Hyperspectral remote sensing of plant pigments. *J. Exp. Bot.* **2006**, *58*, 855–867. [CrossRef]
45. Nagaraja, A.; Sahoo, R.N.; Usha, K.; Singh, S.K.; Sivaramanae, N.; Gupta, V.K. Spectral discrimination of healthy and malformed mango panicles using spectrodariometer. *Indian J. Hortic.* **2014**, *71*, 40–44.
46. Xue, J.; Su, B. Significant Remote Sensing Vegetation Indices: A Review of Developments and Applications. *J. Sens.* **2017**, *2017*, 1353691. [CrossRef]
47. Avtar, R.; Yunus, A.P.; Saito, O.; Kharrazi, A.; Kumar, P.; Takeuchi, K. Multi-temporal remote sensing data to monitor terrestrial ecosystem responses to climate variations in Ghana. *Geocarto Int.* **2020**, 1–17. [CrossRef]
48. Wang, J.; Ding, J.; Yu, D.; Teng, D.; He, B.; Chen, X.; Ge, X.; Zhang, Z.; Wang, Y.; Yang, X.; et al. Machine learning-based detection of soil salinity in an arid desert region, Northwest China: A comparison between Landsat-8 OLI and Sentinel-2 MSI. *Sci. Total Environ.* **2020**, *707*, 136092. [CrossRef] [PubMed]
49. Zeng, L.; Wardlow, B.D.; Wang, R.; Shan, J.; Tadesse, T.; Hayes, M.J.; Li, D. A hybrid approach for detecting corn and soybean phenology with time-series MODIS data. *Remote Sens. Environ.* **2016**, *181*, 237–250. [CrossRef]
50. Hatfield, J.L.; Prueger, J.H. Value of Using Different Vegetative Indices to Quantify Agricultural Crop Characteristics at Different Growth Stages under Varying Management Practices. *Remote Sens.* **2010**, *2*, 562–578. [CrossRef]
51. Suresh, K.; Behera, S.K.; Manorama, K.; Mathur, R.K. Phenological stages and degree days of oil palm crosses grown under irrigation in tropical conditions. *Ann. Appl. Biol.* **2020**, *178*, 121–128. [CrossRef]
52. Sawant, S.A.; Chakraborty, M.; Suradhaniwar, S.; Adinarayana, J.; Durbha, S.S. Time Series Analysis of Remote Sensing Observations for Citrus Crop Growth Stage and Evapotranspiration Estimation. *ISPRS—Int. Arch. Photogramm. Remote Sens. Spat. Inf. Sci.* **2016**, *41*, 1037–1042. [CrossRef]
53. Brinkhoff, J.; Vardanega, J.; Robson, A.J. Land Cover Classification of Nine Perennial Crops Using Sentinel-1 and -2 Data. *Remote Sens.* **2019**, *12*, 96. [CrossRef]
54. Brinkhoff, J.; Robson, A.J. Block-level macadamia yield forecasting using spatio-temporal datasets. *Agric. For. Meteorol.* **2021**, *303*, 108369. [CrossRef]
55. Vayssières, J.F.; Sinzogan, A.; Adandonon, A.; Rey, J.Y.; Dieng, E.O.; Camara, K.; Sangaré, M.; Ouedraogo, S.; Sidibé, A.; Keita, Y.; et al. Annual population dynamics of mango fruit flies (Diptera: Tephritidae) in West Africa: Socio-economic aspects, host phenology and implications for management. *Fruits* **2014**, *69*, 207–222. [CrossRef]

56. Vannière, H.; Rey, J.-Y.; Vayssières, J.-F.; Maraite, H. *Crop Production Protocol—Mango (Mangifera indica)*; PIP: Maastricht, The Netherlands, 2013.
57. DEA. Digital Earth Africa User Guide. Available online: https://docs.digitalearthafrica.org/en/latest/data_specs/Sentinel-2_Level-2A_specs.html (accessed on 2 August 2021).
58. Main-Knorn, M.; Pflug, B.; Louis, J.; Debaecker, V.; Müller-Wilm, U.; Gascon, F. Sen2Cor for sentinel-2. In *Image and Signal Processing for Remote Sensing XXIII*; International Society for Optics and Photonics: Bellingham, WA, USA, 2017; p. 1042704.
59. Obregón, M.Á.; Rodrigues, G.; Costa, M.J.; Potes, M.; Silva, A.M. Validation of ESA Sentinel-2 L2A Aerosol Optical Thickness and Columnar Water Vapour during 2017–2018. *Remote Sens.* **2019**, *11*, 1649. [CrossRef]
60. Gascon, F.; Bouzinac, C.; Thépaut, O.; Jung, M.; Francesconi, B.; Louis, J.; Lonjou, V.; Lafrance, B.; Massera, S.; Gaudel-Vacaresse, A.; et al. Copernicus Sentinel-2A Calibration and Products Validation Status. *Remote Sens.* **2017**, *9*, 584. [CrossRef]
61. Richter, R.; Louis, J.; Müller-Wilm, U. *Sentinel-2 MSI—Level 2A Products Algorithm Theoretical Basis Document*; European Space Agency: Paris, France, 2012; Volume 49, pp. 1–72.
62. Braaten, J.D.; Cohen, W.B.; Yang, Z. Automated cloud and cloud shadow identification in Landsat MSS imagery for temperate ecosystems. *Remote Sens. Environ.* **2015**, *169*, 128–138. [CrossRef]
63. Zekoll, V.; Main-Knorn, M.; Alonso, K.; Louis, J.; Frantz, D.; Richter, R.; Pflug, B. Comparison of Masking Algorithms for Sentinel-2 Imagery. *Remote Sens.* **2021**, *13*, 137. [CrossRef]
64. Zhu, Z.; Wang, S.; Woodcock, C.E. Improvement and expansion of the Fmask algorithm: Cloud, cloud shadow, and snow detection for Landsats 4–7, 8, and Sentinel 2 images. *Remote Sens. Environ.* **2015**, *159*, 269–277. [CrossRef]
65. Rouse, J., Jr.; Haas, R.; Schell, J.; Deering, D. *Monitoring Vegetation Systems in the Great Plains with Erts*; NASA Special Publication: Washington, DC, USA, 1974; Volume 351, p. 309.
66. Gitelson, A.A.; Gritz, Y.; Merzlyak, M.N. Relationships between leaf chlorophyll content and spectral reflectance and algorithms for non-destructive chlorophyll assessment in higher plant leaves. *J. Plant Physiol.* **2003**, *160*, 271–282. [CrossRef] [PubMed]
67. Huete, A.; Didan, K.; Miura, T.; Rodriguez, E.P.; Gao, X.; Ferreira, L.G. Overview of the radiometric and biophysical performance of the MODIS vegetation indices. *Remote Sens. Environ.* **2002**, *83*, 195–213. [CrossRef]
68. Kaufman, Y.J.; Justice, C.O.; Flynn, L.P.; Kendall, J.D.; Prins, E.M.; Giglio, L.; Ward, D.E.; Menzel, W.P.; Setzer, A.W. Potential global fire monitoring from EOS-MODIS. *J. Geophys. Res.* **1998**, *103*, 32215–32238. [CrossRef]
69. Huete, A.R. A soil-adjusted vegetation index (SAVI). *Remote Sens. Environ.* **1988**, *25*, 295–309. [CrossRef]
70. Rahman, M.M.; Robson, A.J. A Novel Approach for Sugarcane Yield Prediction Using Landsat Time Series Imagery: A Case Study on Bundaberg Region. *Adv. Remote Sens.* **2016**, *5*, 93–102. [CrossRef]
71. Vani, V.; Mandla, V.R. Comparative Study of NDVI and SAVI vegetation Indices in Anantapur district semi-arid areas. *Int. J. Civ. Eng. Technol.* **2017**, *8*, 559–566.
72. Wiegand, C.; Gerbermann, A.; Gallo, K.; Blad, B.; Dusek, D. Multisite analyses of spectral-biophysical data for corn. *Remote Sens. Environ.* **1990**, *33*, 1–16. [CrossRef]
73. Wiegand, C.L.; Maas, S.J.; Aase, J.K.; Hatfield, J.L.; Pinter, P.J.; Jackson, R.D.; Kanemasu, E.T.; Lapitan, R.L. Multisite analyses of spectral-biophysical data for wheat. *Remote Sens. Environ.* **1992**, *42*, 1–21. [CrossRef]
74. Yoav, B.; Braun, H.; John, W. Tukey's Contributions to Multiple Comparisons. *Ann. Stat.* **2002**, *30*, 1576–1594. Available online: https://www.jstor.org/stable/1558730 (accessed on 9 November 2021).
75. Vasavada, N. One-Way ANOVA with Post-Hoc Tukey HSD Test Calculator. Available online: https://astatsa.com/OneWay_Anova_with_TukeyHSD/_get_data/ (accessed on 1 July 2021).
76. Jannoyer, M.; Lauri, P.-E. Young Flush Thinning in Mango (cv. Cogshall) Controls Canopy Density and Production. *Acta Hortic.* **2009**, *820*, 395–402. [CrossRef]
77. Solanki, P.; Shah, N.; Sonavane, S.; Prajapati, D. Impact of different pruning time and intensity on vegetative parameters of mango cv. Kesar under high density plantation. *Ecol. Environ. Conserv.* **2014**, *20*, S411–S414.
78. Kouadio, L.; Newlands, N.K.; Davidson, A.; Zhang, Y.; Chipanshi, A. Assessing the Performance of MODIS NDVI and EVI for Seasonal Crop Yield Forecasting at the Ecodistrict Scale. *Remote Sens.* **2014**, *6*, 10193–10214. [CrossRef]
79. Anderson, L.O.; Aragão, L.E.O.C.; Shimabukuro, Y.E.; Almeida, S.; Huete, A. Fraction images for monitoring intra-annual phenology of different vegetation physiognomies in Amazonia. *Int. J. Remote Sens.* **2011**, *32*, 387–408. [CrossRef]
80. Ovakoglou, G.; Alexandridis, T.K.; Clevers, J.G.P.W.; Gitas, I.Z. Downscaling of MODIS leaf area index using landsat vegetation index. *Geocarto Int.* **2020**, 1–24. [CrossRef]
81. Yebra, M.; Van Dijk, A.; Leuning, R.; Huete, A.; Guerschman, J.P. Evaluation of optical remote sensing to estimate actual evapotranspiration and canopy conductance. *Remote Sens. Environ.* **2013**, *129*, 250–261. [CrossRef]
82. Basso, B.; Cammarano, D.; Carfagna, E. Review of Crop Yield Forecasting Methods and Early Warning Systems. In Proceedings of the First Meeting of the Scientific Advisory Committee of the Global Strategy to Improve Agricultural and Rural Statistics, Rome, Italy, 18 July 2013.
83. Sadeh, Y.; Zhu, X.; Dunkerley, D.; Walker, J.P.; Zhang, Y.; Rozenstein, O.; Manivasagam, V.; Chenu, K. Fusion of Sentinel-2 and PlanetScope time-series data into daily 3 m surface reflectance and wheat LAI monitoring. *Int. J. Appl. Earth Obs. Geoinf.* **2020**, *96*, 102260. [CrossRef]